



HAL
open science

The Influence of Slipface Angle on Fluvial Dune Growth

Suleyman Naqshband, David Hurther, S. Giri, R. Bradley, Ray Kostaschuk, J. Venditti, A. J. F. Hoitink

► **To cite this version:**

Suleyman Naqshband, David Hurther, S. Giri, R. Bradley, Ray Kostaschuk, et al.. The Influence of Slipface Angle on Fluvial Dune Growth. *Journal of Geophysical Research: Earth Surface*, 2021, 126 (4), 10.1029/2020JF005959 . hal-03250674

HAL Id: hal-03250674



<https://hal.science/hal-03250674v1>

Submitted on 4 Jun 2021

HAL is a multi-disciplinary open access archive for the deposit and dissemination of scientific research documents, whether they are published or not. The documents may come from teaching and research institutions in France or abroad, or from public or private research centers.

L'archive ouverte pluridisciplinaire **HAL**, est destinée au dépôt et à la diffusion de documents scientifiques de niveau recherche, publiés ou non, émanant des établissements d'enseignement et de recherche français ou étrangers, des laboratoires publics ou privés.



S. Naqshband¹ , D. Hurther², S. Giri³ , R. W. Bradley⁴ , R. A. Kostaschuk⁵ ,
J. G. Venditti^{4,5} , and A. J. F. Hoitink¹ 

Key Points:

- Dune slipface angle adjusts to the imposed flow at time scales similar to the evolution of dune height and length
- The initiation of a flow separation zone intensifies trough scour, and results in acceleration of dune growth
- Sediment transport distributions reveal that bed material avalanche processes over dune lee sides depend on dune slipface angle

Correspondence to:

S. Naqshband,
Suleyman.Naqshband@wur.nl

Citation:

Naqshband, S., Hurther, D., Giri, S., Bradley, R. W., Kostaschuk, R. A., Venditti, J. G., & Hoitink, A. J. F. (2021). The influence of slipface angle on fluvial dune growth. *Journal of Geophysical Research: Earth Surface*, 126, e2020JF005959. <https://doi.org/10.1029/2020JF005959>

Received 30 OCT 2020
Accepted 3 MAR 2021

¹Department of Environmental Sciences, Wageningen University, Wageningen, The Netherlands, ²Laboratory of Geophysical and Industrial Flows (LEGI), CNRS, University Grenoble Alpes, Grenoble, France, ³Department of River Dynamics, Morphology & Inland Shipping, Deltares, Delft, The Netherlands, ⁴Department of Geography, Simon Fraser University, Burnaby, BC, Canada, ⁵School of Environmental Science, Simon Fraser University, Burnaby, BC, Canada

Abstract Dunes dominate the bed of sandy rivers and they respond to flow by changing shape and size, modifying flow, and sediment transport dynamics of rivers. Our understanding of and ability to predict dune adaptation, particularly dune growth and decay, remain incomplete. Here, we investigate dune growth from an initial flatbed in a laboratory setting by continuously mapping the 3D bed topography using a line laser scanner combined with a 3D camera. High-resolution profiles of flow velocity and sediment concentration providing both bedload and suspended sediment fluxes were obtained by deploying Acoustic Concentration and Velocity Profiler technology. Our analysis reveals that the magnitude of the dune slipface angle, which determines flow separation and controls turbulence production, adjusts to the imposed flow at time scales similar to the evolution of dune height and length. The initiation of a flow separation zone intensifies through scour, and results in acceleration of the dune growth. Gradients in sediment transport and the rate of dune growth are inherently linked to spatial variations in slipface angles. During dune growth, the slipface angle evolves differently than the ratio of dune height to length, which immediately reaches its equilibrium value after dune initiation.

1. Introduction

Interaction between a flow field and the underlying sandy bed gives rise to bedform topography over a wide range of spatial and temporal scales. Dunes are the most common and prominent bedforms observed in sandy alluvial systems. They are an important source of flow resistance, generating macroturbulent coherent structures that lead to enhanced dissipation of flow kinetic energy at viscous microscales (e.g., Venditti & Bennet, 2000). In addition, dune development, migration, and growth dominate bedload dynamics in sand-bedded rivers (Frings & Kleinhans, 2008; Gomez et al., 1990; Ma et al., 2017; Venditti et al., 2005a). Dune migration also leaves a characteristic signature in the rock record—cross-stratification—a key building block of alluvial deposits on Earth as well as on other planets (e.g., Best & Fielding, 2019; Ewing et al., 2015; Galeazzi et al., 2018; Leary & Ganti, 2020). Hence, dunes have attracted substantial attention from geomorphologists, sedimentologists, and hydraulic engineers with a rich history of observations from Sorby (1859) and Gilbert (1914) until today.

Research on dunes has considered dune initiation from a flatbed and growth toward a dynamic equilibrium state in steady uniform flows. Theories that explain dune initiation include the generation of bed defects by coherent turbulent flow structures that grow by downstream propagation (e.g., Best, 1992; Grass, 1970; Gyr & Schmidt, 1989; Williams & Kemp, 1971) and instability interface theory that suggests instantaneous generation of bedforms due to an instability formed at the water-sediment interface (Liu, 1957; Venditti et al., 2006). Defect initiation occurs near the threshold of motion for a sand bed while instantaneous initiation occurs when a general motion of a sand bed occurs (Venditti et al., 2005b). Once initiated, dune growth has been explained by invoking hydrodynamic or kinematic processes (Venditti & Bradley, 2020). Gradual dune growth by hydrodynamic processes has been explained with linear stability analyses that involve imposing a spatial lag ϕ between sediment transport maximum and topographic maximum, allowing growth or diminution of initial bed perturbation (e.g., Colombini & Stocchino, 2008; Fredsøe, 1981; Kennedy, 1963; Smith, 1970). Rapid growth by kinematic processes occurs by bedform coalescence to form larger features (Coleman & Melville, 1996; Leary & Ganti, 2020; Martin & Jerolmack, 2013; Myrow et al., 2018; Raudkivi & Witte, 1990). Smaller and faster bedforms merge or amalgamate to form larger, slower migrating dunes.

© 2021. The Authors.

This is an open access article under the terms of the [Creative Commons Attribution-NonCommercial-NoDerivs License](https://creativecommons.org/licenses/by-nc-nd/4.0/), which permits use and distribution in any medium, provided the original work is properly cited, the use is non-commercial and no modifications or adaptations are made.

While existing initiation and growth theories explain how bedforms initiate and grow, they provide little insight into bedform morphology (shape and dimensions) and kinematics (translation and deformation) during growth. Recently, Bradley and Venditti (2019a) used large-scale flume experiments that covered a wide range of flow and sediment transport conditions to show that the process of dune growth from an initial flatbed is more complex than previously conceptualized, and that the functional form of dune growth curves—depicting spatially averaged time evolution of dune height and length—strongly depend on the transport stage applied. In particular, a punctuated growth curve was found for mixed load dominated conditions, with an initial slow linear growth of bedforms followed by a period of exponential growth. The initial growth was attributed to organization of small 2D features which gradually grew into 3D features. It was further suggested that the successive exponential growth phase may be a result of increased trough scour due to enhanced turbulence at the bed, caused by flow separation behind dune lee sides. Although growth curves are prevailing tools that allow prediction of dune dimensions and their response to imposed flows, particularly of importance through passage of a flood wave, their explanatory power of underlying dune growth mechanisms remains limited.

Understanding dune growth requires consideration of turbulent flow fields, dune morphology, sediment transport, and the redistribution of sediment over and among dunes, details of which are not captured by mean geometric parameters such as dune height and length (Parsons & Best, 2013; Reesink et al., 2018). Significant progress has been made into understanding the dynamics of flow separation and eddy generation over fixed and mobile, high-angle dunes (HADs, $\sim 30^\circ$) (e.g., Bourgoin et al., 2020; Dey et al., 2020; Naqshband et al., 2014c, 2017; Omidyeganeh & Piomelli, 2013) and low-angle dunes (LADs, $< 10^\circ$) (e.g., Best & Kostaschuk, 2002; Kwoil et al., 2017; Lefebvre et al., 2016, 2019; Motamedi et al., 2012, 2014; Unsworth et al., 2018). Yet quantitative observations and simulations of sediment fluxes along migrating and changing dune forms remain extremely rare (Naqshband et al., 2014b, 2014c, 2017). Consequently, we lack insight into sediment erosional and depositional processes causing dune adaptation (changes in dune morphology and kinematics) to imposed flows. More specifically, there is no mechanistic explanation of how changes in a turbulent flow field associated with changes in dune morphology—most notably dune slipface slope—result in sediment transport gradients along dune beds, and how this spatiotemporal variation in sediment flux contributes to dune growth. Herein, dune slipface slope refers to the steepest segment of a dune lee side.

Here, we investigate dune growth from an initial flatbed in a shallow laboratory flume by continuously mapping 3D bed topography as it evolved toward a dynamic equilibrium. High-resolution sediment flux profiles referenced to the exact measured position of the bed were obtained by deploying an advanced hydroacoustic flow instrumentation known as the Acoustic Concentration and Velocity Profiler (ACVP). Our analysis demonstrates how sediment transport gradients and the rate of dune growth are associated with spatial variation in dune slipface angles, paving the way for understanding and predicting of form-related components of shear stress and flow resistance, and ultimately river morphodynamics. We show that the dune slipface angle progresses similarly to dune height during dune growth, as opposed to the dune steepness, which reaches its equilibrium value immediately after initiation.

2. Methods and Experimental Conditions

Experiments were carried out at the Kraijenhoff van de Leur laboratory for Water and Sediment Dynamics, Wageningen University & Research. A 1.2-m wide and 14.4-m long flume was used, focusing on an effective measuring section of 4 m. The slope of the flume can be accurately adjusted up to 4% (Figure 1). Both water and sediment were recirculated, with a fine-meshed filter mounted at the downstream end of the flume, guaranteeing full recirculation of the mobile sediment load. Our experimental design, procedure, and instrumentation are briefly outlined below. For more specific details of our methodology and experimental techniques see Naqshband et al. (2017) and Naqshband and Hoitink (2020).

To investigate dune growth and adaptation, a 15-cm thick layer of uniformly distributed, lightweight polystyrene particles was installed as a surrogate for sand after Naqshband and Hoitink (2020). This allowed dynamic similarity of both flow characteristics (Froude number) and sediment transport conditions (Shields number) between our shallow laboratory flows and rivers that are an order of magnitude deeper. The bed

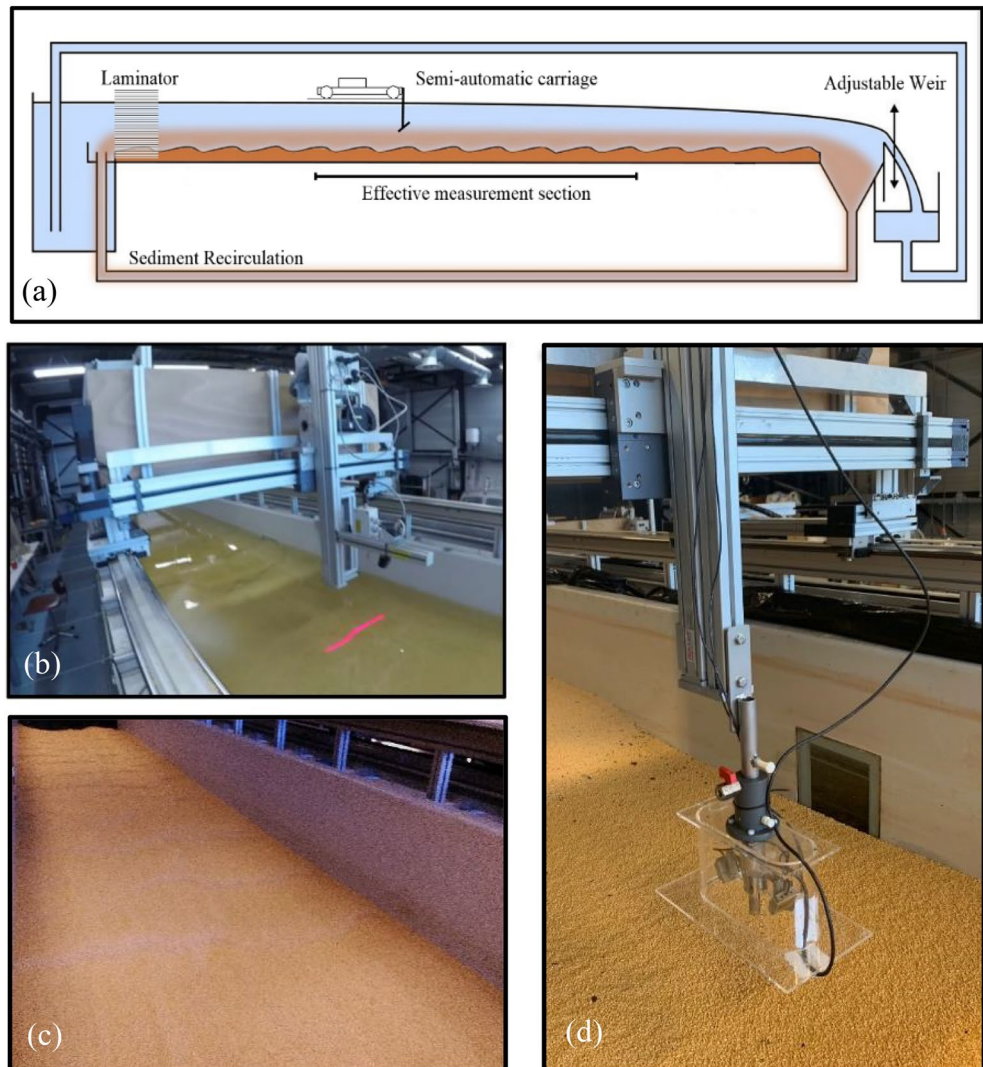


Figure 1. Overview of the experimental setup, (a) side view of the tilting flume with the effective measurement section between $x = 4$ m and $x = 8$ m in streamwise direction, (b) positioning of the line laser scanner on a semiautomatic carriage, (c) fully developed equilibrium dunes, and (d) setup of the Acoustic Concentration and Velocity Profiler (ACVP, see Naqshband et al., 2014b for details).

was flattened and the flume was slowly filled with water from both the upstream and downstream ends, preventing significant bed disturbance. A predefined flow discharge, flume slope, and water depth were chosen to represent a mixed load dominated (MLD) transport condition (Table 1), with both bedload and suspended load transport. The water surface slope adjusted to the imposed mean bed slope while reaching a dynamic equilibrium in which dunes were not systematically growing or shrinking. Flow discharge was continuously measured with an electromagnetic flow meter, and water levels were monitored at four positions using evenly spaced stilling wells along the centerline of the flume. The effective measurement section of the flume bed ($x = 4$ m to $x = 8$ m) was continuously scanned along a 0.51 m center strip ($y = 0.35$ m to $y = 0.86$ m) with a streamwise resolution of 2 mm and a crosswise resolution of 3 mm, over a period of ~ 8 h with an average time interval of 12.5 min between consecutive scans. This continuous bed level monitoring was carried out using a line laser scanner combined with a 3D camera using the methods in de Ruijsscher et al. (2018). As the line laser scanner is not submerged in water, bed elevation is measured without disturbing the flow field and underlying bed morphology. Each bed scan consists of 167 evenly spaced parallel transects over the 0.51-m wide strip. Distribution of bedform dimensions (dune height Δ , length λ , and slipface angle α) was obtained from these transects using a frequently applied bedform tracking tool (van der Mark

Table 1
Overview of Flow, Sediment, and Dune Bed Characteristics

Parameter	Value
Discharge, Q ($\text{m}^3 \text{s}^{-1}$)	0.050
Water depth, H (m)	0.25
Flume slope, $S \times 10^{-3}$ (-)	1.0
Mean bulk velocity, U (m s^{-1})	0.17
Froude number, Fr (-)	0.11
Bed shear stress, τ_b (Pa)	1.73
Bed shear velocity, u_* (m s^{-1})	0.04
Suspension number, u_*/w_s (-)	1.43
Shields number, θ (-)	1.53
Transport stage, θ/θ_c (-)	47.8
Mean particle diameter, $D_{50} \times 10^{-2}$ (m)	0.21
Sediment density, ρ_s (kg m^{-3})	1,055
Settling velocity, w_f (m s^{-1})	0.029
Critical Shields number, θ_c (-)	0.032
Static angle of repose ^a , β ($^\circ$)	24.0
Particle roundness ^b , R (-)	0.46
Particle sphericity ^c , S (-)	0.81
Dune height in equilibrium, Δ_e (m)	0.083
Dune length in equilibrium, Λ_e (m)	1.43
Migration velocity in equilibrium, $C_e \times 10^{-4}$ (m s^{-1})	5.33
Dune steepness, Δ_e/Λ_e (-)	0.058
Dune slipface angle in equilibrium, α_e ($^\circ$)	19.8
Time needed for equilibrium, T_e (min)	125

^aStatic angle of repose of polystyrene particles is determined using the fixed funnel method according to Al-Hashemi and Al-Amoudi (2018).

^bParticle roundness quantifies the sharpness of particle corners calculated after the method described by Zheng and Hryciw (2015) and Hryciw et al. (2016). ^cParticle sphericity is the ratio of particle width to particle length.

et al., 2008). For each bed scan, spatially averaged bedform dimensions presented in this study are computed by averaging over 167 transects. The outlined experimental procedure was repeated to investigate the reproducibility of these experiments, and to quantify the spatiotemporal variation of dune dimensions during dune growth from an initial flatbed.

In a successive experiment under the exact same flow and sediment condition, sediment flux profiles were measured over the entire flow depth, over a period of 125 min (time needed to reach a dynamic equilibrium starting from an initial flatbed, T_e [min] in Table 1). Direct sediment flux profiles in horizontal and vertical directions were obtained using the ACVP as described by Hurther et al. (2011). It provides quasi-instantaneous, simultaneous, and colocated vertical profiles of the two-component velocity field (streamwise u and vertical w) together with the acoustic intensity profiles referenced to the exact location of the undisturbed bed level (using the Acoustic Bed Interface Tracking method of Hurther and Thorne [2011]), with a spatial and temporal resolution of 1.5 mm and 1/70 s, respectively. The acoustic intensity profiles are transformed into sediment mass concentration profiles by applying dual frequency inversion methods and incoherent scattering theory to polystyrene particles (Hurther et al., 2011; Thorne & Hurther, 2014). Compared to the well-known implicit iterative and the explicit inversions, this technique offers the unique advantage of being unaffected by the nonlinear sediment attenuation effect across highly concentrated flow regions (Hurther et al., 2011). The polystyrene bed interface and the interface between the suspended load and the bedload are determined by identifying, in the backscattered signal profile, the nonmoving bed echo characterized by its immobility and the echo from the suspended sediment concentration, respectively. These two near-bed echoes can be separated when the acoustic intensity profile is derived from the demodulated Doppler signals since the acoustic scatters constituting the nonmoving polystyrene bed produce a constant voltage with negligible signal variance. This results in the time evolution of the nonmoving polystyrene bed, the overlaying high sediment concentration layer (the bed load layer), and the suspended load layer including both the two-component flow velocity and the sediment concentration (Fromant et al., 2019; Naqshband et al., 2014b, 2017). The ACVP was mounted on a measurement carriage and positioned at a fixed location along the flume ($x = 6$ m, see Figure 1d) with dunes migrating underneath. ACVP data presented herein are time-averaged over

a period of 10 s. This averaging period was chosen such to obtain a stable convergent mean vertical velocity profile along the dune bed. During this averaging period, bed displacement was negligible compared to dune length (maximum bed displacement of 0.5 cm for an equilibrium dune length of 1.43 m, Table 1). An equivalent distance is also shown which is derived by transforming ACVP measurement time series into streamwise distance along the flume, using mean bed displacement inferred from equilibrium bedform migration velocity (Table 1).

The ACVP technology was previously used to investigate the contribution of both bedload and suspended load to migrating sand dunes in equilibrium (Naqshband et al., 2014c), to quantify sediment transport distribution during dune transition to upper stage plane bed (Naqshband et al., 2017), and to study boundary layer flow and sediment transport dynamics under gravity current-driven and wave-driven sheet flows (Fromant et al., 2018, 2019; Revil-baudard et al., 2015, 2016). In the present study, we deploy the ACVP to investigate dynamics of flow separation in the dune lee side and associated sediment transport gradients during dune growth from an initial flatbed. This will provide quantitative knowledge of the mechanisms governing dune adaptation and will facilitate more accurate predictions of form-related components of shear stress and flow resistance, which are crucial components in modeling sediment transport and river morphology.

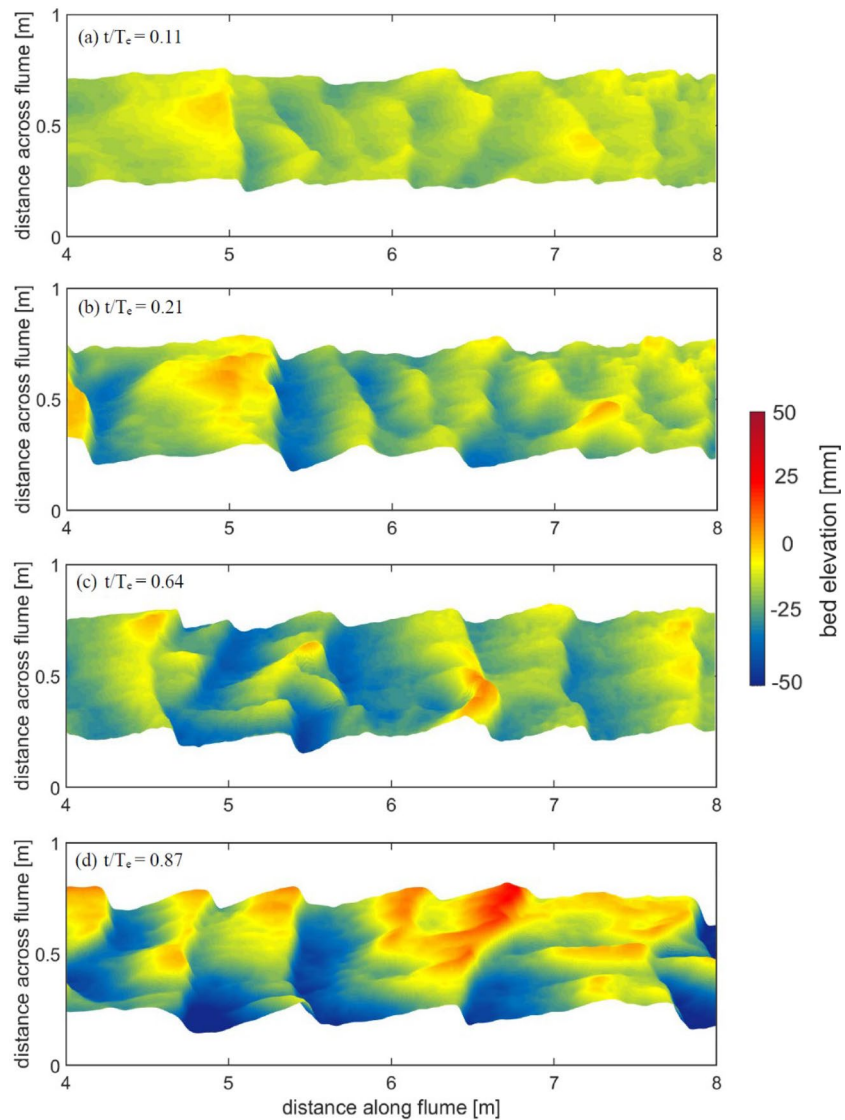


Figure 2. Different stages of bed morphology illustrating dune growth from an initial flatbed toward a dynamic equilibrium with fully developed dunes, time evolves from top to bottom, with T_c the time needed to reach a dynamic equilibrium from an initial flatbed.

3. Results

3.1. Dune Growth From an Initial Flatbed

Measured bed topography illustrates successive stages of dune development and growth toward a dynamic equilibrium (Figure 2). Small bedforms instantaneously appeared over the entire bed as soon as water flow began (Figure 2a). The initial growth phase is characterized by 3D irregular features (Figure 2b) that grew and merged into larger 2D bedforms (Figure 2c). Superimposed bedforms were also observed on dune stoss slopes, causing additional events of dune splitting and merging, observed in previous research (Carling et al., 2000; Leary & Ganti, 2020; Reesink et al., 2018; Venditti et al., 2005a, 2016). Soon after, however, bedform spurs (ridges parallel to the mean flow direction, Figure 2c) appeared, transforming dune crestlines back to 3D (Swanson et al., 2017). During the second, more rapid dune growth phase, dunes became higher and longer with deeper scours in their troughs (Figure 2d). Trough scouring continued during the third growth stage reaching a dynamic equilibrium.

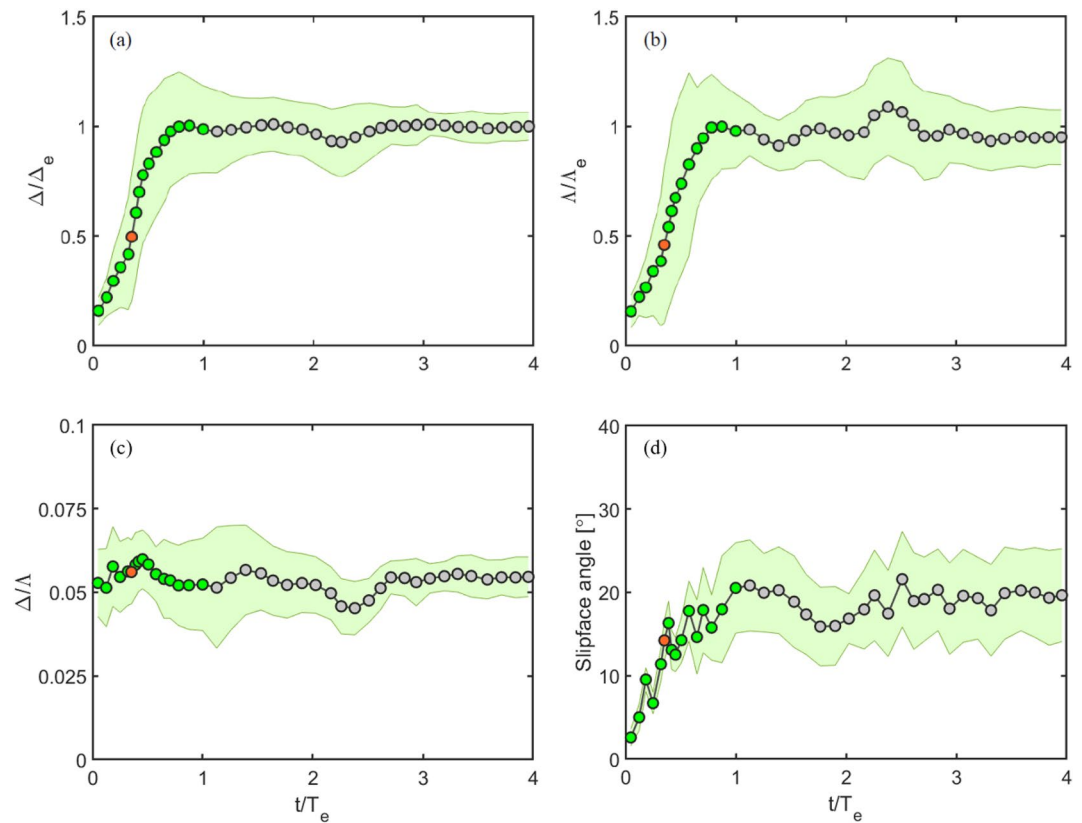


Figure 3. Morphological growth curves showing the evolution of dune dimensions over time, (a) relative dune height (Δ/Δ_e), (b) relative dune length (Λ/Λ_e), (c) dune steepness (Δ/Λ), and (d) dune slipface angle. T_e is the time needed to reach a dynamic equilibrium from an initial flatbed, shaded green area is mean values \pm standard deviation. Red circles in (a) to (c) indicate the moment of transition between a linear and an exponential growth, which coincides with the time that the onset angle for initiation of flow separation is exceeded, indicated with red circle in (d).

Dune growth curves show initial linear growth followed by a period of exponential growth after $t/T_e = 0.35$ (red circle in Figure 3). Topographic variability in dune height (mean \pm standard deviation) increased during the growth stage but decreased and remained constant after reaching a dynamic equilibrium (Figure 3a).

Dune lengths had larger and fairly constant relative variability over the entire duration of the experiment as in previous research (Naqshband et al., 2014a; Venditti et al., 2016). Dune steepness varied through time, but showed no systematic change as the dunes grew (Figure 3c). The time evolution of spatially averaged dune slipface angles had a rapid initial increase followed by a more gradual increase toward equilibrium (Figure 3d). Variability in dune slipface angles remained large after reaching equilibrium. Ultimately, the evolution of dune slipface angles revealed that as the onset angle for initiation of flow separation (predicted to equal 11° by Lefebvre and Winter [2016]) is exceeded (red circle in Figure 3d) and trough scour is intensified, less sediment bypasses the flow reattachment point, and consequently, more sediment arriving at the dune crest is maintained within the dune, accelerating its growth. Dune slipface angle distributions change during dune growth toward dynamic equilibrium (Figure 4). During the initial stage of dune development, distributions are positively skewed toward lower slipface angles with mean values deviating from the corresponding modes (Figure 4a and 4b). In the equilibrium phase, distributions are near-Gaussian (Figure 4c and 4d).

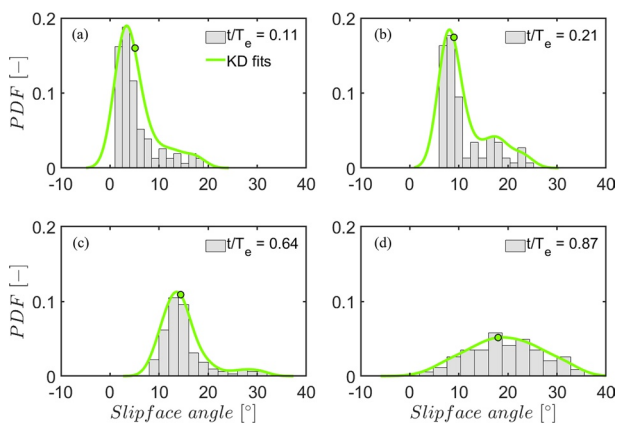


Figure 4. Distribution of dune slipface angle at four different stages of dune development as shown in Figure 1. The solid green lines represent kernel density fits to dune slipface data with circles indicating spatially averaged values.

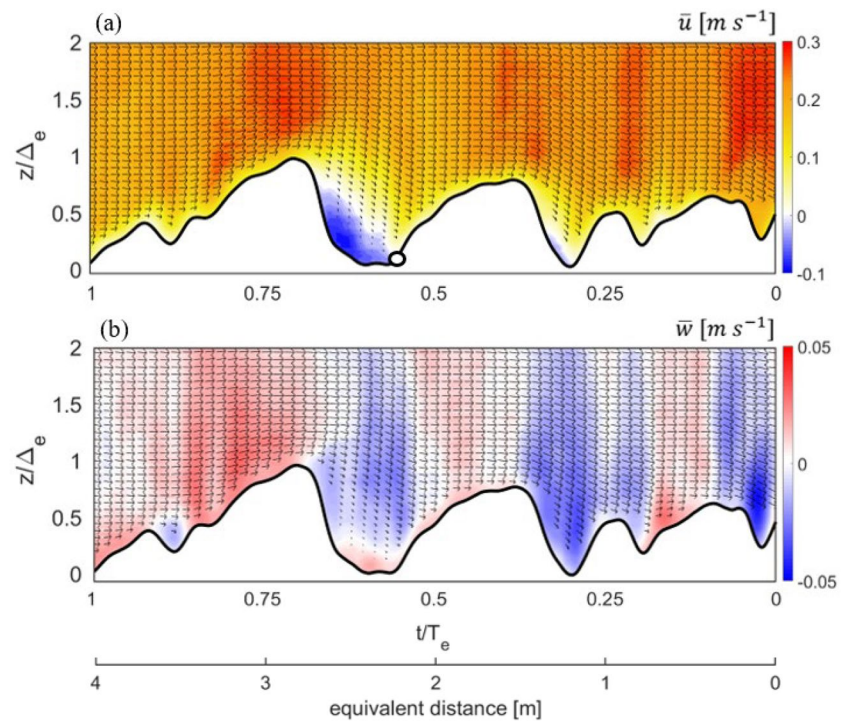


Figure 5. Flow field over mobile dunes, with (a) mean streamwise flow velocity and (b) mean vertical flow velocity. Arrows represent the mean velocity vector field $\bar{v}_{u,w}$. Flow direction is from left to right with measured dune profile in solid black line. Open black circle indicates the location of flow reattachment point. An equivalent distance is derived from transforming ACVP measurement time series into streamwise distance along the flume, using mean bed displacement (see Section 2). ACVP, Acoustic Concentration and Velocity Profiler.

3.2. Flow Field, Sediment Concentration, and Sediment Flux

Measured flow fields over growing dunes reveal distinct flow patterns caused by topographic forcing (Figure 5). During the initial growth stage with relatively small dunes and low slipface angles, the flow pattern is characterized by a strong downslope near-bed current and gentle vertical gradients, with a maximum flow velocity over the dune trough. Recent work by Kostaschuk and Venditti (2019) showed that a strong downslope current over dune lee side is associated with LADs, and that these currents transport large amounts of sediment ultimately contributing to the generation of small-scale, migrating, superimposed bedforms on dune lee sides. As dunes grow in size and their slipface angles increase, the downslope current decreases in strength and a zone of flow separation starts to develop with reversed near-bed flow, vertical gradients become more distinct, and the location of maximum flow velocity shifts upstream toward the dune crest. In the second stage of dune growth toward equilibrium, a shear layer developed and the flow separation zone further expanded, with more pronounced negative near-bed velocities (e.g., Kwoil et al., 2016; Naqshband et al., 2014c). The mean distance from the separation point to the flow reattachment point (indicated with open circles in Figure 5), the flow separation length, is found to be 3–4 times the equilibrium dune height Δ_e , which is in good agreement with values reported in previous studies (e.g., Paarlberg et al., 2007). The exact location of the flow reattachment point at the bed is the boundary between the negative and the positive mean streamwise flow velocities (Naqshband et al., 2014c).

The evolution of the flow field results in a characteristic sediment concentration pattern over the dune bed (Figure 6a), with sediment concentration just above the undisturbed bed level (detected with the ABIT method of Hurther and Thorne [2011]) equal to the granular bed density $\rho_s(1-\epsilon)=633 \text{ (kg m}^{-3}\text{)}$ where ($\rho_s=1,055 \text{ (}\rho_s=1,055 \text{ (kg m}^{-3}\text{))}$ is sediment density, and $\epsilon=0.4 \text{ (-)}$ is granular bed porosity). The highest concentrations are observed close to the bed, with peaks in suspended sediment over the dune stoss, at the dune crest, and over the dune lee side during the initial growth phase. With initiation and

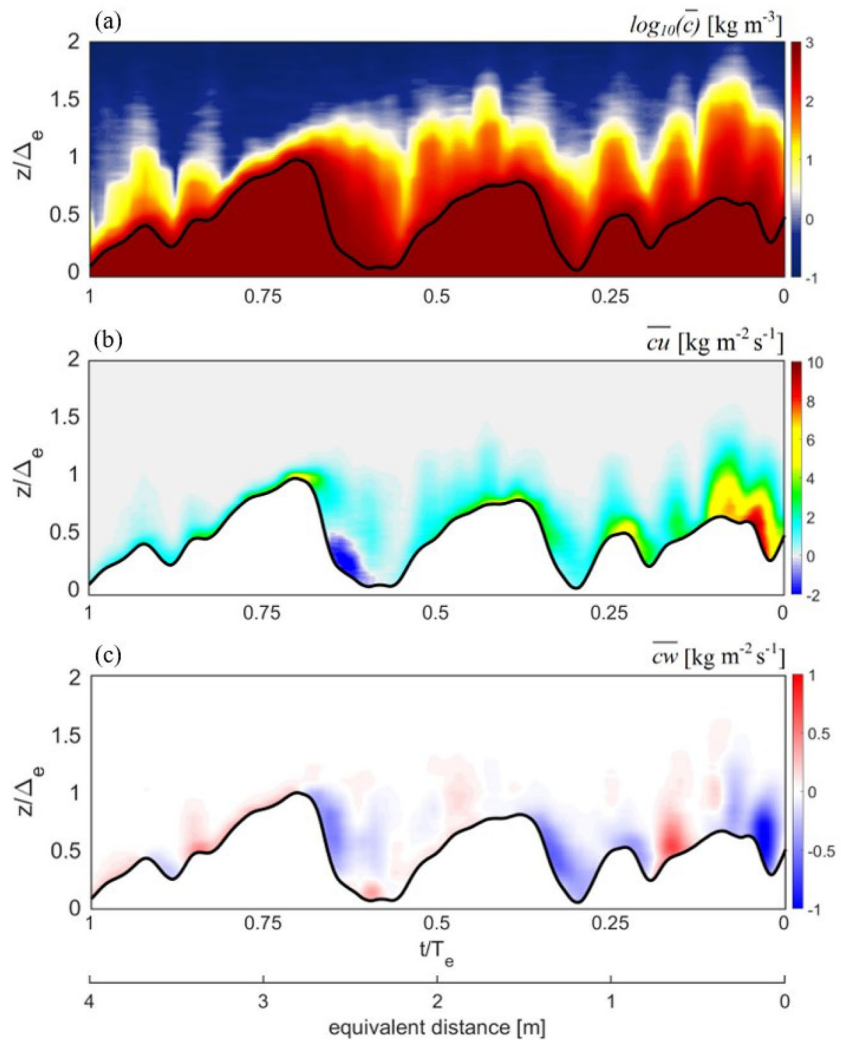


Figure 6. Sediment concentration and fluxes over mobile dunes, with (a) mean sediment concentration, (b) mean streamwise sediment flux, and (c) mean vertical sediment flux. Solid black line is the measured dune profile.

expansion of flow separation in the second stage of dune growth, peaks in suspended sediment concentration were observed over the dune trough due to flow deceleration and the associated turbulence production, with smaller suspension peaks caused by turbulent bursts that result from shear layer vortices impacting the dune bed at $t/T_e = 0.92$. As the mean flow reattaches at the bed and the bed shear stress becomes practically zero at the flow reattachment point, a strong decrease in sediment concentration is observed at this location.

The product of flow velocity and sediment concentration gives the sediment flux (i.e., mean streamwise $\bar{c}u$ and mean vertical $\bar{c}w$ sediment fluxes in Figure 6b and 6c, respectively). Gradients in those fluxes ultimately drive local changes in dune morphology and dune interaction. During the initial growth stage, with relatively small dunes and low slipface angles, the largest streamwise fluxes are encountered at the dune crest and over the dune lee side. As dunes evolve and become larger toward equilibrium, with increased slipface angles, $\bar{c}u$ decreases over the dune lee sides and eventually becomes negative due to flow separation and the upslope current. Larger slipface angles are associated with weaker downslope near-bed currents (Best & Kostaschuk, 2002; Kostaschuk & Venditti, 2019; Kwohl et al., 2016, 2017), which results in less pronounced (negative) downward vertical flux $\bar{c}w$ over dune lee sides. The observed pattern in $\bar{c}u$ further reveals a discontinuity over the dune trough at $t/T_e = 0.55$, which corresponds to the location of the flow reattachment point with zero net sediment flux.

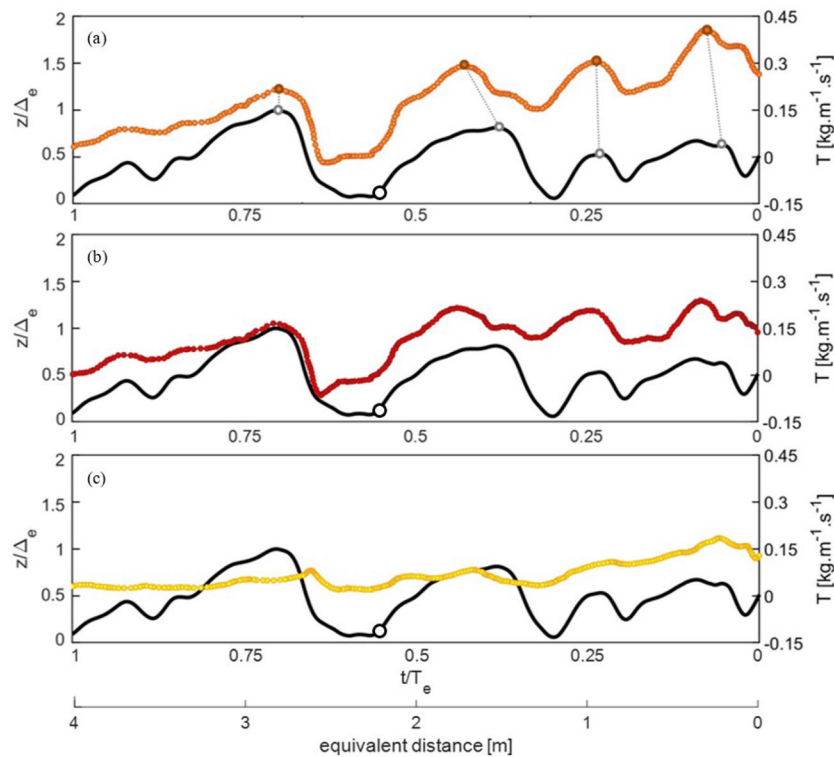


Figure 7. Sediment transport distribution over mobile dunes, with (a) showing total load, (b) bedload, and (c) suspended load transport. Solid black line is the measured dune profile, with black open circle the location of flow reattachment point. Orange circles in (a) indicate the location of dune-maximum sediment transport, relative to dune topographic maximum (open gray circle).

3.3. Sediment Transport Dynamics

Integration of mean streamwise flux profiles over the entire flow depth H gives the distribution of total sediment transport per unit channel width along the migrating dune bed (Figure 7a). Although sediment transport is usually considered as a steady flux calculated using reach-averaged flow conditions, it is clear that sediment fluxes vary with topography. Bedload (Figure 7b) varies with topography more than suspended load (Figure 7c). As such, bedload variation controls the depth-integrated sediment flux. Consequently, dune morphology (shape and dimensions) is set by bedload fluxes under the considered transport stage. The combination of small dunes that possess low slipface angles associated with a strong downslope near-bed current, and high sediment concentration over their crest and lee side, results in the largest sediment transport rates observed during the initial stage of dune growth. As dunes grow in size and their slipface angles increase, the contribution of form-related flow resistance becomes larger, reducing sediment transport capacity of the flow (e.g., Kwoil et al., 2017; Lefebvre et al., 2016; Ma et al., 2017). This is reflected in a decrease of both dune-averaged as well as dune-maximum sediment transport rates over the course of dune growth.

The sediment transport distribution further illustrates distinct avalanching processes of bed material over dune lee sides. In the presence of a flow separation zone associated with steep slipface angles, avalanching is characterized by an immediate decay of bedload transport over the dune lee side, reaching zero transport just ahead of the flow reattachment point. In absence of a flow separation zone throughout the initial stage of dune growth, avalanching is more gradual, with sediment being deposited over dune lee sides and much further into dune troughs.

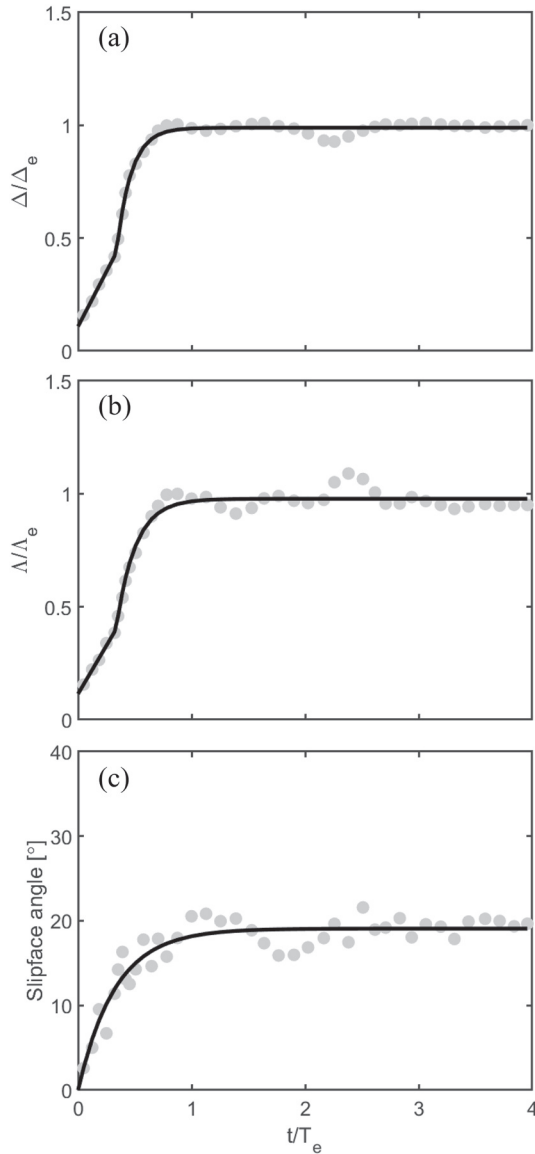


Figure 8. Growth curve fits through time with (a) height, (b) length, and (c) slipface angle. (a) and (b) display punctuated growth, where a period of linear growth is followed by exponential growth, while (c) shows only exponential growth (see Table 2 for model fitting results).

4. Discussion

4.1. Dune Slipface Angle and Flow Separation

Existing dune growth curves exclusively consider the time evolution of dune height and length from an initial flatbed toward a fully developed equilibrium dune field (e.g., Baas, 1999; Bradley & Venditti, 2019a; Colombini & Stocchino, 2008; Coleman et al., 2005; Iseya, 1984; Nikora & Hicks, 1997; Venditti et al., 2005a). Dune slipface angles—determinative for flow separation and turbulence production—are often assumed to instantaneously reach high angles sloping at the angle of repose ($\sim 30^\circ$). Our experimental study with lightweight polystyrene grains allow for dune morphodynamic similarity between shallow laboratory flow conditions and rivers that are an order of magnitude deeper (Naqshband & Hoitink, 2020). We show that dune slipface angles adjust to the imposed flow at time scales similar to the evolution of dune height and length (Figure 3d). Although HADs with steep slipfaces at the angle of repose that produce a permanent zone of flow separation are characteristic for shallow laboratory flows, such steep slipface angles are an exception for our shallow flow dunes, analogous to observed slipface angles of dunes in deeper rivers (e.g., Cisneros et al., 2020; Galeazzi et al., 2018; Kostaschuk & Villard, 1999; McLean & Smith, 1979).

Using high-resolution numerical modeling, Lefebvre (2019) showed that the size of the flow separation zone and magnitude of reversed flow, in addition to the magnitude of the slipface angle, is controlled by slipface orientation relative to the mean flow direction. For a slipface orientation $>25^\circ$ compared to the main flow direction, a strong cross-stream current develops, suppressing turbulence, and reversed flow. Previous work has also shown that sediment is dispersed in the cross-stream direction in the presence of dunes, which become more pronounced when dunes have a 3D character (Allen, 1982; Parsons et al., 2005; Reesink et al., 2018). By quantifying particle hop distance and travel time over equilibrium mobile dunes, Ashley et al. (2020) showed that dunes significantly increase mean and standard deviation of cross-stream hop distances relative to a flatbed. As flow and sediment data in our study is limited to 2D slices through dunes which possess a 3D character from time to time, care must be taken while using this data as reference for modeling flow and sediment transport processes.

4.2. Mechanisms of Dune Growth

The evolution of a bedform field from a flatbed has been shown to display exponential growth at lower transport stages (e.g., Baas et al., 1999; Bradley & Venditti, 2019a; Venditti et al., 2005a) and punctuated growth, when a period of initially linear growth is abruptly interrupted by exponential growth, at higher transport stages (Bradley & Venditti, 2019a). Exponential growth is expressed as

$$\Delta = a_\Delta \left(1 - e^{-b_\Delta t}\right), \quad (1a)$$

$$\Lambda = a_\Lambda \left(1 - e^{-b_\Lambda t}\right), \quad (1b)$$

where a_Δ and a_Λ are asymptotes that describe equilibrium height and length, respectively, and b_Δ and b_Λ are growth constants. The dune height and length growth curves observed in these experiments (Figure 8a

Table 2
Model Fitting Results

Dune property	Growth phase						Equilibrium dimension (m, °)	T_{efit} (hr)
	Linear		Phase end (hr)	Exponential				
	Slope (–)	Intercept (m)		a (m, °)	b (–)	R^2 (–)		
Height	0.0394	0.00890	0.650	0.0404	3.86	0.97	0.0811	1.91
Length	0.669	0.181	0.650	0.819	2.94	0.92	1.54	2.28
Slipface angle	—	—	—	19.1	1.51	0.90	19.1	3.05

Exponential phase results are from fits using Equation 1. Equilibrium dimensions are the asymptotes in Equation 1 plus the dimensions at the end of the linear growth phase. Following Baas (1994), Venditti et al. (2005b), and Bradley and Venditti (2019b), T_{efit} is the time required for the growth curve to reach 99% of the asymptote.

and 8b) show punctuated growth. Growth curves are marked by a linear phase of relatively slower growth as bedforms initially evolve from the flatbed until they reach a height where exponential growth occurs. In our experiments, the linear growth phase is interrupted by exponential growth when $t/T_e = 0.35$ (Figure 3). Exponential model fit results (Table 2) show that dune height reaches equilibrium slightly faster than dune length.

Bradley and Venditti (2019a) argued that the linear phase of growth is punctuated because there is a shift in the mode of sediment transport. During the linear phase, nascent bedforms grow to exceed a critical height where they can no longer be contained in the near-bed flow layer. Growth then shifts to exponential as intense scour in troughs leads to more rapid bedform growth. These morphodynamics are likely responsible for the height and length growth curves observed in Figure 8. The Bradley and Venditti (2019a) observation of punctuated growth were limited to flow depths <0.20 m and θ/θ_c conditions up to values of 21.2. Beyond this transport stage, growth appeared instantaneous because it happened too quickly so that it was difficult to confirm the form of the growth curves. These observations at a flow depth of 0.25 m with lower density material suggests that punctuated growth occurs at a higher transport stage ($\theta/\theta_c = 47.8$, see Table 1) than observed by Bradley and Venditti (2019a).

The slipface angle growth curve shows purely exponential growth without an initial linear phase expressed as

$$\alpha = a_\alpha \left(1 - e^{-b_\alpha t}\right), \quad (2)$$

where a_α describes the equilibrium slipface angle and b_α is a growth constant. The slipface angle evolution to equilibrium lags behind dune height and length (Table 2).

Explaining dune growth by hydrodynamic processes requires imposing a spatial lag between bedload transport maximum and topographic maximum, yet, demonstration that the physical lags are real has proven challenging (cf. McLean, 1990; Venditti, 2013). Smith (1970) argued that if maximum sediment transport is located upstream of the dune crest, then sediment deposition will occur on the dune crest and dunes will grow larger. If the sediment transport maximum is downstream of dune crest, then the dune crest will erode resulting in dune decay. If sediment transport maximum is in-phase with the topographic maximum, dunes will migrate downstream without changing shape and dimension. The measured sediment transport distribution over dunes in the present study reveals—for the first time—an upstream spatial lag between dune crest and maximum sediment transport which appears to vary significantly with evolution phases (Figure 7a). This lag becomes more pronounced as the onset angle for initiation of flow separation is exceeded during the second stage of dune growth, with sediment being eroded from the dune stoss, and deposited on dune crest and lee side, resulting in dune growth. Closer to equilibrium the lag disappears and the sediment flux maximum coincides with the topographic maximum. This is when sediment deposition on dune stoss and crest is balanced by sediment erosion along these locations. As a result, dune height and length stabilize, which is also reflected in a gradual decrease in growth rates toward the upper asymptote

(Figure 3a and 3b). Future research should address the detailed causes of variability in the observed spatial lag, to provide a better basis for its use in numerical bedform evolution models (e.g., Giri & Shimizu, 2006; Naqshband et al., 2016; Nelson et al., 2008; Shimizu et al., 2009; Van Duin et al., 2017).

4.3. Low-Angle Dune Formation

The rapid decay in bedload transport rates over the dune lee sides necessarily leads to oversteepening of the upper slope and avalanching on the slipface. Slipface angles in this study can be compared to the two types of avalanching processes proposed by Kostaschuk and Venditti (2019) to explain why deep (>2.5 m) rivers have low-angle dunes on their beds. Theoretical and experimental analysis has indicated that granular avalanches composed of sand are unlikely to flow on gradients <24° (Cassar et al., 2005). Kostaschuk and Venditti (2019) use this criterion to separate small high-angle dunes found in flumes and shallow rivers from larger, low-angle dunes in deeper flows. Low-angle slipfaces <24° are maintained by a combination of liquefied avalanches capable of transporting sediment over longer distances and at lower angles than granular avalanches, and downslope currents that transport bedload over the lee side when flow separation becomes intermittent or absent. Mean slipface angles for the dunes in this study increase from around 2° to 18° during the initial stage of dune growth to around 19.8° for equilibrium dunes (Figure 3d and Table 1). Extremes above the mean reach 27° for equilibrium dune slipfaces, but most are below 24°, making them low-angle dunes.

Application of the Wallis-Lowe liquefaction model (see Kostaschuk & Venditti, 2019 for details) allows us to determine if the low lee angles are maintained by liquefied avalanches. The model assumes that, at the instant of liquefaction in a deposit, the particles are supported by excess pore pressure and the fractional particle concentration (volume of sediment/total volume) of the dispersion is constant with a concentration C_0 . As pore pressures decline, the particles settle to the bed in a simple two-layer resedimentation process where the interface between the dispersed grains at C_0 and the resedimented grains, at a higher concentration C_1 , rises at a uniform velocity. Resedimentation is complete when the interface between the overlying clear water and the liquefied dispersion coincides with the surface of the resedimented grains. Complete resedimentation of the dispersion occurs over a time t_r :

$$t_r = \frac{\zeta(C_1 - C_0)}{C_1 w_d \cos \alpha}, \quad (3)$$

where ζ is the initial thickness of the deposit, α is slipface angle, $w_d = w_f(1 - C_0)^n$ is the aggregate fall velocity of the dispersion, w_f is the fall velocity of a single particle, and n is an empirically derived coefficient. For the simplest case of laminar flow and no interaction between the liquefied grains, the maximum distance traveled by the flow is $\Gamma = \text{truh}$, where $uh = 0.7\sqrt{(\delta\rho_{1-f} / \rho_1)gY}$ is the slope-parallel velocity of the head of the flow, ρ_{1-f} is the density difference between the liquefied avalanche ρ_l and the overlying fluid ρ_f , and Y is the thickness of the head. We assume characteristic values (see Lowe, 1976: cgs units are used herein to maintain consistency with empirical constants in the model) of $C_0 = 0.54$, $C_1 = 0.6$, $n = 4.7$ and $g = 981 \text{ cm s}^{-2}$. The settling velocity for the polystyrene particles is measured as $w_f = 2.9 \text{ cm s}^{-1}$ (Table 1). Application of the model requires an estimate of the initial thickness of the triangular wedge deposit. Flume experiments have shown that slipface avalanches result from the failure of triangular-shaped wedges at the top of the slipface that are 10–20% of dune height (e.g., Reesink & Bridge, 2007; Venditti et al., 2005b). Following Kostaschuk and Venditti (2019), we assume a rectangular deposit thickness of 5–10% of dune height (1/2 the maximum triangular wedge thickness).

Kostaschuk and Venditti (2019) calculated values of $\Gamma SI = 0.29\text{--}0.83$ (S_l is slipface length) for a small high-angle sand dune comparable in size to the equilibrium dunes in this study, 0.59–1.51 for a large low-angle dune in the rock record (Røe, 1987) and 0.55–1.46 for a large low-angle dune in the Fraser River. When $\Gamma SI > 1$, liquefied avalanches can travel the whole length of the slipface and therefore exert a first order control on the slipface angle. When $\Gamma SI < 1$, liquefied flows would be confined to the upper slipface and would then have to fail as granular avalanches dominated by grain-to-grain contacts. Table 3 summarizes the values of parameters in the Wallis-Lowe model as applied to the equilibrium dunes in this study. Comparison of the predicted maximum liquefied avalanche travel distances Γ with respect to the measured length of

Table 3
Parameters for the Wallis-Lowe Model

Parameter	Value
Initial deposit thickness, ζ (cm)	0.42–0.84
Slipface angle, α ($^{\circ}$)	19.8
Density of liquefied avalanche, ρ_l (g cm^{-3})	1.03
Density of water, ρ_f (g cm^{-3})	1.00
Avalanche head velocity, u_h (cm s^{-1})	2.40–3.41
Avalanche head thickness, Y (cm)	0.42–0.84
Resedimentation time, t (s)	0.56–1.12
Liquefied avalanche travel distance, Γ (cm)	1.34–3.88
Slipface length, S_l (cm)	11.25

the slipface S_l shows that the putative liquefied avalanche would travel a fractional distance along the slipface of $\Gamma S_l = 0.12\text{--}0.34$. This suggests that the dune slipface angles in this study are not controlled by liquefied avalanches, and are instead controlled by granular avalanches. The Wallis-Lowe model is principally derived for granular sand avalanches. Since polystyrene particles have different inertial properties compared to sand grains, additional experimental testing may be required to further explore these avalanches.

Our results suggest that low lee angles may be maintained without liquefied avalanches, and the specific reasons why lee side angles in the lightweight sediments remain low are not immediately obvious. Polystyrene granular avalanches may be able to travel on lower gradients compared to granular avalanches of quartz density sand particles. The static angle of repose in water of the polystyrene particles is 24° (Table 1). The dynamic angle of repose is generally $3\text{--}10^{\circ}$ lower than the static angle (Al-Hashemi & Al-Amoudi, 2018), which is consistent with the avalanche slipface angles of the equilibrium polystyrene dunes herein (Table 2). In

addition, the angle of repose is affected by particle shape, increasing with deviations from roundness and sphericity (Al-Hashemi & Al-Amoudi, 2018). The measurements of roundness ($R = 0.46$) and sphericity ($S = 0.81$) of the polystyrene particles show that the particles can be classified as subrounded (Hryciw et al., 2016), which would result in steeper slipface angles compared to round and spherical particles of the same density (Al-Hashemi & Al-Amoudi, 2018). Combined, the effects of relative sediment density and roundness on the angle of repose produce low-angle dunes in our experiments without the liquefied avalanches described by Kostaschuk and Venditti (2019) over dunes in deep rivers. We expect that experiments with rounder and more spherical polystyrene particles would allow exploration of dunes with even lower slipface angles.

While the experiments suggest that lightweight sediments cannot be used to explore the liquefied avalanches that dominate low lee angles in deep rivers, the particles do produce dunes similar to those formed in deep rivers. This provides an opportunity to investigate flow dynamics, roughness, and form drag of actively migrating LADs at laboratory scale. The experiments also point to other mechanisms that may control low lee angles for dunes close to the threshold value estimated as 24° , such as dunes observed in the Río Paraná, Argentina ($\alpha \sim 15^{\circ}\text{--}24^{\circ}$; Parsons et al., 2005). The relative density of sediment evidently plays an important role in the emergence of low lee angles, a phenomenon not readily evident for dunes formed in water flows on Earth because there is so little variation in the relative density of sediment.

4.4. Implications for Modeling Dune Morphodynamics and Flow Resistance

These experimental findings are useful to get insight into sediment transport processes associated with bedform growth that, in turn, could be used to verify and improve the approach and performance of numerical models. Physics-based morphological models are increasingly used to simulate bedform morphodynamics. The models range from simple to complex in terms of both hydrodynamics and sediment transport (Giri & Shimizu, 2006; Goll, 2017; Khosronejad & Sotiropoulos, 2014; Lefebvre & Winter, 2016; Nabi et al., 2014, 2015; Niemann et al., 2010; Paarlberg et al., 2009; Shimizu et al., 2009; Sun & Xiao, 2016; Tjerry & Fredsøe, 2005; Uchida & Fukuoka, 2013; van Duin et al., 2017; Yamaguchi et al., 2020). Most of these models include a parameterized spatial lag between sediment transport maximum and topographic maximum. This parameterization is either based on (i) an equilibrium transport approach with incorporation of local bed slope effects, (ii) a nonequilibrium sediment transport relation using pick-up and deposition functions that requires information on particle step lengths, or (iii) a (linear) relaxation equation that describes the response of bedform geometry to changes in flow. One of the fundamental challenges is to replicate the interaction between flow, sediment transport, and morphology physically reliably. The question regarding which approach replicates physically correct sediment transport and morphological processes associated

with bedform growth remains ambiguous. Given the fact that the sediment transport formulations, used in most of the numerical models, are empirical or semiempirical, it is rather difficult to capture the physics of sediment transport associated with bedform initiation and growth processes.

Our experimental findings shed some light on these underlying processes, revealing spatial lag between sediment transport and bed morphology at different stages of dune growth. The observed variation in this spatial lag is similar to findings from a numerical dune evolution model with nonequilibrium sediment transport formulation in Yamaguchi et al. (2020). The experimental results also highlight the sediment transport processes over the lee side of the dunes, which include both the distribution of bed and suspended sediment transport. Another important outcome of the experiment is the lower slipface angle, which could be useful for verifying numerical models, since they usually predict higher slipface angles close to the angle of repose. The model concept of a bed slope effect used to simulate dune evolution and growth even requires an avalanche function of sediment load over dune lee side, to restrict the lee side angle to the angle of repose. This should be explored in a future study with the numerical model including similar lightweight materials as used in current experiments.

The experimental findings presented herein can be employed for detailed exploration and verification of different sediment transport approaches in numerical models. This will help to further verify model performance, as well as to improve fundamental aspects of sediment transport approaches in numerical models. Another important aspect is the accurate prediction of form drag exerted by bedforms. The numerical model must be verified for the case when the slipface angle is lower than the angle of repose. Consequently, it is necessary to explore the evolution of form drag and its effect on water surface, particularly for the case with a lower slipface angle as found in these experiments and in the field. Physical experiments and numerical modeling can be combined to develop a generic method for assessing flow resistance.

5. Conclusions

Flume experiments were designed to study dune adaptation to an imposed flow, and in particular the mechanics of dune growth. The 3D bed topography was continuously monitored using a line laser scanner combined with a camera. High-resolution profiles of flow velocity and sediment concentration, providing direct estimations of both the bedload and the suspended load sediment flux, were obtained by deploying an Acoustic Concentration and Velocity Profiler. The main findings of our study are summarized as follows:

1. Dune slipface angles—determinative for flow separation and turbulence production—adjust to the imposed flow at time scales similar to the evolution of dune height and length
2. The evolution of dune slipface angles reveals that as the onset angle for initiation of flow separation is exceeded, and trough scour is intensified, less sediment bypasses the flow reattachment point. This accelerates dune growth as more sediment arriving at the dune crest is maintained within the dune
3. The sediment transport distribution illustrates distinct avalanching processes of bed material over dune lee sides. The avalanching is characterized by an immediate decay of bedload transport over the dune lee side in the presence of a flow separation zone. In absence of a flow separation zone, avalanching is more gradual, with sediment being deposited over dune lee sides and much further into dune troughs.

Data Availability Statement

The data used in this manuscript are archived and made publicly available through the 4TU.Centre for Research Data (S. Naqshband 2021: supporting information for the publication: The influence of slipface angle on dune growth. 4TU.ResearchData. Dataset. <https://doi.org/10.4121/13625735.v1>).

References

- Al-Hashemi, H. M. B., & Al-Amoudi, O. S. B. (2018). A review on the angle of repose of granular materials. *Powder Technology*, 330, 397–417. <https://doi.org/10.1016/j.powtec.2018.02.003>
- Allen, J. R. L. (1982). Sedimentary structures, their character and physical basis. In *Developments in sedimentology 30 a and b* (Vol. 1–2). Amsterdam: Elsevier Scientific Publishing Company.

Acknowledgments

This research was funded by the Netherlands Organisation for Scientific Research (NWO), within Vici project “Deltas out of shape: regime changes of sediment dynamics in tide-influenced deltas” (Grant NWO-TTW 17062), and the Dutch Ministry of Infrastructure and Environment (Rijkswaterstaat, Fund 5160957319). ACVP technology development by D. Hurther is supported by the French DGA-funded ANR Astrid Maturation project MESURE (ANR-16-ASMA-0005-01).

- Ashley, T. C., Mahon, R. C., Naqshband, S., Leary, K. P., & McElroy, B. (2020). Probability distributions of particle hop distance and travel time over equilibrium mobile bedforms. *Journal of Geophysical Research: Earth Surface*, *125*, e2020JF005647. <https://doi.org/10.1029/2020JF005647>
- Baas, J. H. (1994). A flume study on the development and equilibrium morphology of current ripples in very fine sand. *Sedimentology*, *41*(2), 185–209. <https://doi.org/10.1111/j.1365-3091.1994.tb01400.x>
- Baas, J. H. (1999). An empirical model for the development and equilibrium morphology of current ripples in fine sand. *Sedimentology*, *46*(1), 123–138. <https://doi.org/10.1046/j.1365-3091.1999.00206.x>
- Best, J. L. (1992). On the entrainment of sediment and initiation of bed defects: Insights from recent developments within turbulent boundary layer research. *Sedimentology*, *39*(5), 797–811. <https://doi.org/10.1111/j.1365-3091.1992.tb02154.x>
- Best, J. L., & Fielding, C. R. (2019). Describing fluvial systems: Linking processes to deposits and stratigraphy (Vol. 488). London: Geological Society, Special Publications.
- Best, J. L., & Kostaschuk, R. A. (2002). An experimental study of turbulent flow over a low-angle dune. *Journal of Geophysical Research*, *107*(C9), 3135. <https://doi.org/10.1029/2000JC000294>
- Bourgoin, A., Guillou, S. S., Thiebot, J., & Ata, R. (2020). Use of Large-Eddy Simulation for the bed shear stress estimation over a dune. *International Journal of Sediment Research*. <https://doi.org/10.1016/j.ijsrc.2019.10.002>
- Bradley, R. W., & Venditti, J. G. (2019a). The growth of dunes in rivers. *Journal of Geophysical Research: Earth Surface*, *124*, 548–566. <https://doi.org/10.1029/2018JF004832>
- Bradley, R. W., & Venditti, J. G. (2019b). Transport scaling of dune dimensions in shallow flows. *Journal of Geophysical Research: Earth Surface*, *124*, 526–547. <https://doi.org/10.1029/2018JF004832>
- Carling, P. A., Golz, E., Orr, H. G., & Radecki-Pawlik, A. (2000). The morphodynamics of fluvial sand dunes in the River Rhine, near Mainz, Germany. I. Sedimentology and morphology. *Sedimentology*, *47*, 227–252.
- Cassar, C., Nicolas, N., & Pouliquen, O. (2005). Submarine granular flows down inclined planes. *Physics of Fluids*, *17*, 103301. <https://doi.org/10.1063/1.2069864>
- Cisneros, J., Best, J., van Dijk, T., de Almeida, R. P., Amsler, M., Boldt, J., et al. (2020). Dunes in the world's big rivers are characterized by low-angle lee-side slopes and a complex shape. *Nature Geoscience*, *13*, 156–162. <https://doi.org/10.1038/s41561-019-0511-7>
- Coleman, S. E., & Melville, B. W. (1996). Initiation of bedforms on a flat sand bed. *Journal of Hydraulic Engineering*, *122*, 301–310.
- Coleman, S. E., Zhang, M. H., & Clunie, T. M. (2005). Sediment-wave development in subcritical water flow. *Journal of Hydraulic Engineering*, *131*(2), 106–111. [https://doi.org/10.1061/\(ASCE\)0733-9429\(2005\)131:2\(106\)](https://doi.org/10.1061/(ASCE)0733-9429(2005)131:2(106))
- Colombini, M., & Stocchino, A. (2008). Finite-amplitude river dunes. *Journal of Fluid Mechanics*, *611*, 283–306.
- deRuijsscher, T. V., Hoitink, A. J. F., Dinnissen, S., Vermeulen, B., & Hazenberg, P. (2018). Application of a line laser scanner for bedform tracking in a laboratory flume. *Water Resources Research*, *54*, 2078–2094. <https://doi.org/10.1002/2017WR021646>
- Dey, S., Paul, P., Fang, H., & Padhi, E. (2020). Hydrodynamics of flow over two-dimensional dunes. *Physics of Fluids*, *32*, 025106. <https://doi.org/10.1063/1.5144552>
- Ewing, R. C., Hayes, A. G., & Lucas, A. (2015). Sand dune patterns on Titan controlled by long-term climate cycles. *Nature Geoscience*, *8*, 15–19.
- Fredsoe, J. (1981). Unsteady flow in straight alluvial streams. Part 2. Transition from dunes to plane bed. *Journal of Fluid Mechanics*, *102*, 431–453. <https://doi.org/10.1017/S0022112081002723>
- Frings, R. M., & Kleinhans, M. G. (2008). Complex variations in sediment transport at three large river bifurcations during discharge waves in the river Rhine. *Sedimentology*, *55*(5), 1145–1171. <https://doi.org/10.1111/j.1365-3091.2007.00940.x>
- Fromant, G., Hurther, D., van der Zanden, J., van der A, D. A., Cáceres, I., O'Donoghue, T., & Ribberink, J. S. (2019). Wave boundary layer hydrodynamics and sheet flow properties under large-scale plunging-type breaking waves. *Journal of Geophysical Research: Oceans*, *124*, 75–98. <https://doi.org/10.1029/2018JC014406>
- Fromant, G., Mieras, R. S., Revil-Baudard, T., Puleo, J. A., Hurther, D., & Chauchat, J. (2018). On bedload and suspended load measurement performances in sheet flows using acoustic and conductivity profilers. *Journal of Geophysical Research: Earth Surface*, *123*, 2546–2562. <https://doi.org/10.1029/2017JF004560>
- Galeazzi, C. P., Almeida, R. P., Mazoca, C. E. M., Best, J. L., Freitas, B. T., Ianniruberto, M., et al. (2018). The significance of superimposed dunes in the Amazon River: Implications for how large rivers are identified in the rock record. *Sedimentology*, *65*, 2388–2403.
- Gilbert, G. K. (1914). *The transport of debris by running water*. US Geological Survey Professional Paper No. 86, 1–263.
- Giri, S., & Shimizu, Y. (2006). Numerical computation of sand dune migration with free surface flow. *Water Resources Research*, *42*, W10422. <http://dx.doi.org/10.1029/2005WR004588>
- Goll, A. (2017). *3D numerical modelling of dune formation and dynamics in inland waterways*. Complete reprint of the Ph.D. thesis, approved by the École doctorale Sciences, Ingénierie et Environnement of the Université Paris-Est, École du Pont-ParisTech.
- Gomez, B., Hubbell, D. W., & Stevens, H. H. (1990). At-a-point bed load sampling in the presence of dunes. *Water Resources Research*, *26*, 2717–2731.
- Grass, A. J. (1970). Initial instability of fine bed sand. *Journal of Hydraulic Engineering*, *96*(3), 619–632.
- Gyr, A., & Schmidt, A. (1989). The different ripple formation mechanism. *Journal of Hydraulic Research*, *27*(1), 61–74. <https://doi.org/10.1080/00221688909499244>
- Hryciw, R. D., Zheng, J., & Shetler, K. (2016). Particle roundness and sphericity from images of assemblies by chart estimates and computer methods. *Journal of Geotechnical and Geoenvironmental Engineering*, *142*, 04016038. [https://doi.org/10.1061/\(ASCE\)GT.1943-5606.0001485](https://doi.org/10.1061/(ASCE)GT.1943-5606.0001485)
- Hurther, D., & Thorne, P. D. (2011). Suspension and near-bed load sediment transport processes above a migrating, sand-rippled bed under shoaling waves. *Journal of Geophysical Research*, *116*, C07001. <https://doi.org/10.1029/2010JC006774>
- Hurther, D., Thorne, P. D., Bricault, M., Lemmin, U., & Barnoud, J. M. (2011). A multi-frequency Acoustic Concentration and Velocity Profiler (ACVP) for boundary layer measurements of fine-scale flow and sediment transport processes. *Coastal Engineering*, *58*, 594–605.
- Iseya, F. (1984). *An experimental study of dune development and its effect on sediment suspension: Environmental Research Center Papers No. 5* (p. 46). Ibaraki, Japan: Environmental Research Center, The University of Tsukuba.
- Kennedy, J. F. (1963). The mechanics of dunes and anti-dunes in erodible bed channels. *Journal of Fluid Mechanics*, *16*, 521–544.
- Khosronejad, A., & Sotiropoulos, F. (2014). Numerical simulation of sand waves in a turbulent open channel flow. *Journal of Fluid Mechanics*, *753*, 150–216.
- Kostaschuk, R. A., & Venditti, J. G. (2019). Why do large, deep rivers have low-angle dune beds? *Geology*, *47*(10), 919–922. <https://doi.org/10.1130/G46460.1>

- Kostaschuk, R. A., & Villard, P. V. (1999). *Turbulent sand suspension over dunes*. In N. D. Smith, & J. Rogers (Eds.), *Fluvial sedimentology VI* (Vol. 28, pp. 3–14). Special Publications of the International Association of Sedimentology.
- Kwoll, E., Venditti, J. G., Bradley, R. W., & Winter, C. (2016). Flow structure and resistance over subaqueous high- and low-angle dunes. *Journal of Geophysical Research: Earth Surface*, *121*, 545–564. <https://doi.org/10.1002/2015JF003637>
- Kwoll, E., Venditti, J. G., Bradley, R. W., & Winter, C. (2017). Observations of coherent flow structures over subaqueous high- and low-angle dunes. *Journal of Geophysical Research: Earth Surface*, *5*, 2244–2268. <https://doi.org/10.1002/2017JF004356>
- Leary, K. C. P., & Ganti, V. (2020). Preserved fluvial cross strata record bedform disequilibrium dynamics. *Geophysical Research Letters*, *47*, e2019GL085910. <https://doi.org/10.1029/2019GL085910>
- Lefebvre, A. (2019). Three-dimensional flow above river bedforms: Insights from numerical modeling of a natural dune field (Río Paraná, Argentina). *Journal of Geophysical Research: Earth Surface*, *124*, 2241–2264. <https://doi.org/10.1029/2018JF004928>
- Lefebvre, A., Paarlberg, A. J., & Winter, C. (2016). Characterising natural bedform morphology and its influence on flow. *Geo-Marine Letters*, *36*, 379–393.
- Lefebvre, A., & Winter, C. (2016). Predicting bedform roughness: The influence of lee side angle. *Geo-Marine Letters*, *36*, 121–133.
- Liu, H. K. (1957). Mechanics of sediment-ripple formation. *Journal of Hydraulics Division, ASCE*, *83*(HY2), 1–23.
- Lowe, D. R. (1976). Subaqueous liquefied and fluidized sediment flows and their deposits. *Sedimentology*, *23*, 285–308. <https://doi.org/10.1111/j.1365-3091.1976.tb00051.x>
- Ma, H., Nittrouer, J. A., Naito, K., Fu, X., Zhang, Y., Moodie, A. J., et al. (2017). The exceptional sediment load of fine-grained dispersal systems: Example of the Yellow River, China. *Science Advances*, *3*(5), e1603114.
- Martin, R. L., & Jerolmack, D. J. (2013). Origin of hysteresis in bed form response to unsteady flows. *Water Resources Research*, *49*, 1314–1333. <https://doi.org/10.1002/wrcr.20093>
- McLean, S. R. (1990). The stability of ripples and dunes. *Earth-Science Reviews*, *29*, 131–144.
- McLean, S. R., & Smith, J. D. (1979). Turbulence measurements in the boundary layer over a sand wave field. *Journal of Geophysical Research*, *84*, 7791–7808.
- Motamedi, A., Afzalimehr, H., Gallichand, J., & Abadi, E. F. N. (2012). Lee angle effects in near bed turbulence: An experimental study on low and sharp angle dunes. *International Journal of Hydraulic Engineering*, *1*, 68–74.
- Motamedi, A., Afzalimehr, H., Zenz, G., & Galoie, M. (2014). RANS simulations of flow over dunes with low lee and sharp lee angles. In P. Gourbesville, J. Cunge, & G. Caignaert (Eds.), *Advances in hydroinformatics* (pp. 525–533). Singapore: Springer.
- Myrow, P. M., Jerolmack, D. J., & Perron, J. T. (2018). Bedform disequilibrium. *Journal of Sedimentary Research*, *88*(9), 1096–1113.
- Nabi, M., Giri, S., Iwasaki, T., Kimura, I., & Shimizu, Y. (2014). Multi-scale modelling of river morphodynamics. In *Proceedings of river flow-2014, Lausanne, Switzerland*.
- Nabi, M., Kimura, I., Hsu, S. M., Giri, S., & Shimizu, Y. (2015). Computational modeling of dissipation and regeneration of fluvial sand dunes under variable discharges. *Journal of Geophysical Research: Earth Surface*, *120*, 1390–1403. <https://doi.org/10.1002/2014JF003364>
- Naqshband, S., & Hoitink, A. J. F. (2020). Scale-dependent evanescence of river dunes during discharge extremes. *Geophysical Research Letters*, *47*, e2019GL085902. <https://doi.org/10.1029/2019GL085902>
- Naqshband, S., Hoitink, A. J. F., McElroy, B., Hurther, D., & Hulscher, S. J. M. H. (2017). A sharp view on river dune transition to upper stage plane bed. *Geophysical Research Letters*, *44*, 11437–11444. <https://doi.org/10.1002/2017GL075906>
- Naqshband, S., Ribberink, J. S., & Hulscher, S. J. (2014a). Using both free surface effect and sediment transport mode parameters in defining the morphology of river dunes and their evolution to upper stage plane beds. *Journal of Hydraulic Engineering*, *140*, 06014010.
- Naqshband, S., Ribberink, J. S., Hurther, D., Barraud, P. A., & Hulscher, S. J. M. H. (2014b). Experimental evidence for turbulent sediment flux constituting a large portion of the total sediment flux along migrating sand dunes. *Geophysical Research Letters*, *41*, 8870–8878. <https://doi.org/10.1002/2014GL062322>
- Naqshband, S., Ribberink, J. S., Hurther, D., & Hulscher, S. J. M. H. (2014c). Bed load and suspended load contributions to migrating sand dunes in equilibrium. *Journal of Geophysical Research: Earth Surface*, *119*, 1043–1063. <https://doi.org/10.1002/2013JF003043>
- Naqshband, S., van Duin, O. J. M., Ribberink, J. S., & Hulscher, S. J. M. H. (2016). Modelling river dune development and dune transition to upper stage plane bed. *Earth Surface Processes and Landforms*, *41*, 323–335. <https://doi.org/10.1002/esp.3360>
- Nelson, J. M., Logan, B. L., Kinzel, P. J., Shimizu, Y., Giri, S., Shreve, R. L., & McLean, S. R. (2008). Bedform response to flow variability. In *Proceedings marine sand-wave and river dune dynamics, MARID, April 2008, Leeds, UK* (pp. 241–248).
- Niemann, S. L., Fredsoe, J., & Jacobsen, N. G. (2010). Sand dunes in steady flow at low Froude numbers: Dune height evolution and flow resistance. *Journal of Hydraulic Engineering, ASCE*, *137*(1), 5–14.
- Nikora, V. I., & Hicks, D. M. (1997). Scaling relationships for sand wave development in unidirectional flow. *Journal of Hydraulic Engineering, ASCE*, *123*(12), 1152–1156. [https://doi.org/10.1061/\(ASCE\)0733-9429\(1997\)123:12\(1152\)](https://doi.org/10.1061/(ASCE)0733-9429(1997)123:12(1152))
- Omidyeganeh, M., & Piomelli, U. (2013). Large-eddy simulation of three-dimensional dunes in a steady, unidirectional flow. Part 2. Flow structures. *Journal of Fluid Mechanics*, *734*, 509–534.
- Paarlberg, A. J., Dohmen-Janssen, C. M., Hulscher, S. J. M. H., & Termes, P. (2007). A parameterization of flow separation over subaqueous dunes. *Water Resources Research*, *43*, W12417. <https://doi.org/10.1029/2006WR005425>
- Paarlberg, A. J., Dohmen-Janssen, C. M., Hulscher, S. J. M. H., & Termes, P. (2009). Modeling river dune evolution using a parameterization of flow separation. *Journal of Geophysical Research*, *114*, F01014. <https://doi.org/10.1029/2007JF000910> ISSN 1048-0227.
- Parsons, D. R., & Best, J. L. (2013). Bedforms: Views and new perspectives from the third international workshop on Marine and River Dune Dynamics (MARID3). *Earth Surface Processes and Landforms*, *38*(3), 319–329. <https://doi.org/10.1002/esp.3360>
- Parsons, D. R., Best, J. L., Orfeo, O., Hardy, R. J., Kostaschuk, R., & Lane, S. N. (2005). Morphology and flow fields of three-dimensional dunes, Río Paraná, Argentina: Results from simultaneous multibeam echo sounding and acoustic Doppler current profiling. *Journal of Geophysical Research*, *110*, F04S03. <https://doi.org/10.1029/2004JF000231>
- Raudkivi, A., & Witte, H. H. (1990). Development of bed features. *Journal of Hydraulic Engineering ASCE*, *116*(9), 1063–1079. [https://doi.org/10.1061/\(ASCE\)0733-9429\(1990\)116:9\(1063\)](https://doi.org/10.1061/(ASCE)0733-9429(1990)116:9(1063))
- Reesink, A. J., Parsons, D., Ashworth, P., Best, J., Hardy, R., Murphy, B., et al. (2018). The adaptation of dunes to changes in river flow. *Earth-Science Reviews*, *185*, 1065–1087. <https://doi.org/10.1016/j.earscirev.2018.09.002>
- Reesink, A. J. H., & Bridge, J. S. (2007). Influence of superimposed bedforms and flow unsteadiness on formation of cross strata in dunes and unit bars. *Sedimentary Geology*, *202*, 281–296. <https://doi.org/10.1016/j.sedgeo.2007.02.005>
- Revil-Baudard, T., Chauchat, J., Hurther, D., & Barraud, P.-A. (2015). Investigation of sheet-flow processes based on novel acoustic high-resolution velocity and concentration measurements. *Journal of Fluid Mechanics*, *767*, 1–30. <https://doi.org/10.1017/jfm.2015.23>
- Revil-Baudard, T., Chauchat, J., Hurther, D., & Eiff, O. (2016). Turbulence modifications induced by the bed mobility in intense sediment laden flows. *Journal of Fluid Mechanics*, *808*, 469–484. <https://doi.org/10.1017/jfm.2016.671>

- Røe, S. L. (1987). Cross-strata and bedforms of probable transitional dune to upper-stage plane-bed origin from a late Precambrian fluvial sandstone, northern Norway. *Sedimentology*, *34*, 89–101. <https://doi.org/10.1111/j.1365-3091.1987.tb00562.x>
- Shimizu, Y., Giri, S., Yamaguchi, I., & Nelson, J. (2009). Numerical simulation of dune-flat bed transition and stage-discharge relationship with hysteresis effect. *Water Resources Research*, *45*, W04429. <https://doi.org/10.1029/2008WR006830>
- Smith, J. D. (1970). Stability of a sand bed subjected to a shear flow of low Froude Number. *Journal of Geophysical Research*, *75*, 5928–5940.
- Sorby, H. C. (1859). On the structures produced by the currents during the deposition of stratified rocks. *Geologist*, *2*, 137–147.
- Sun, R., & Xiao, H. (2016). CFD-DEM simulations of current-induced dune formation and morphological evolution. *Advances in Water Resources*, *92*, 228–239.
- Swanson, T., Mohrig, D., Kocurek, G., Perillo, M., & Venditti, J. (2017). Bedform spurs: A result of a trailing helical vortex wake. *Sedimentology*, *65*, 191–208.
- Thorne, P. D., & Hurther, D. (2014). An overview on the use of backscattered sound for measuring suspended particle size and concentration profiles in non-cohesive inorganic sediment transport studies. *Continental Shelf Research*, *73*, 97–118. <https://doi.org/10.1016/j.csr.2013.10.017>
- Tjerry, S., & Fredsøe, J. (2005). Calculation of dune morphology. *Journal of Geophysical Research*, *110*, F04013. <https://doi.org/10.1029/2004JF000171>
- Uchida, T., & Fukuoka, S. (2013). Quasi 3D numerical simulation for flow and bed variation with various sand waves. In Fukuoka, et al. (Ed.), *Advances in river sediment research* (pp. 221–229). London: Taylor and Francis Group (ISBN: 978-1-138-00062-9).
- Unsworth, C. A., Parsons, D. R., Hardy, R. J., Reesink, A. J. H., Best, J. L., Ashworth, P. J., & Keevil, G. M. (2018). The impact of nonequilibrium flow on the structure of turbulence over river dunes. *Water Resources Research*, *54*, 6566–6584. <https://doi.org/10.1029/2017WR021377>
- Vander Mark, C. F., Blom, A., & Hulscher, S. J. (2008). Quantification of variability in bedform geometry. *Journal of Geophysical Research*, *113*, F03020. <https://doi.org/10.1029/2007JF000940>
- vanDuin, O. J. M., Hulscher, S. J. M. H., Ribberink, J. S., & Dohmen-Janssen, C. M. (2017). Modeling of spatial lag in bed-load transport processes and its effect on dune morphology. *Journal of Hydraulic Engineering*, *143*(2), 04016084. [https://doi.org/10.1061/\(ASCE\)HY.1943-7900.0001254](https://doi.org/10.1061/(ASCE)HY.1943-7900.0001254)
- Venditti, J. G. (2013). Bedforms in sand-bedded rivers. In J. Shroder Jr, & E. Wohl (Eds.), *Treatise on geomorphology* (pp. 137–162). San Diego, CA: Academic Press.
- Venditti, J. G., & Bennett, S. J. (2000). Spectral analysis of turbulent flow and suspended sediment transport over fixed dunes. *Journal of Geophysical Research*, *105*, 22035–22047.
- Venditti, J. G., & Bradley, R. W. (2020). Bedforms in sand bed rivers. *Treatise on Geomorphology*, *9*, 2020. <https://doi.org/10.1016/B978-0-12-409548-9.12519-9>
- Venditti, J. G., Church, M., & Bennett, S. J. (2005a). Morphodynamics of small-scale superimposed sand waves over migrating dune bedforms. *Water Resources Research*, *41*, W10423. <https://doi.org/10.1029/2004WR003461>
- Venditti, J. G., Church, M., & Bennett, S. J. (2005b). On the transition between 2D and 3D dunes. *Sedimentology*, *52*(6), 1343–1359. <https://doi.org/10.1111/j.1365-3091.2005.00748.x>
- Venditti, J. G., Church, M., & Bennett, S. J. (2006). On interfacial instability as a cause of transverse subcritical bedforms. *Water Resources Research*, *42*, W07423. <https://doi.org/10.1029/2005WR004346>
- Venditti, J. G., Lin, C.-Y. M., & Kazemi, M. (2016). Variability in bedform morphology and kinematics with transport stage. *Sedimentology*, *63*, 1017–1040.
- Williams, P. B., & Kemp, P. H. (1971). Initiation of ripples on a flat sand bed. *Journal of Hydraulic Division, ASCE*, *97*, 505–522.
- Yamaguchi, S., Giri, S., Shimizu, Y., & Nelson, J. M. (2020). Morphological computation of dune evolution with equilibrium and non-equilibrium sediment-transport models. *Water Resources Research*, *55*, 8463–8477. <https://doi.org/10.1029/2018WR024166>
- Zheng, J., & Hryciw, R. D. (2015). Traditional soil particle sphericity, roundness and surface roughness by computational geometry. *Géotechnique*, *65*, 494–506. <https://doi.org/10.1680/geot.14.P.192>